arXiv:cond-mat/9603003v1 1 Mar 1996

A self consistent field approach to surfaces of compressible polymer blends

F. Schmid
Johannes Gutenberg Universität Mainz
D55099 Mainz
Germany

Abstract -
A self consistent field theory for compressible polymer mixtures is developed by introducing elements of classical density functional theory into the framework of the Helfand theory. It is then applied to study free surfaces of binary (A,B) polymer blends. Density profiles in the one- and two-phase region are calculated as well as chain end distributions and chain orientations of the minority and the majority component. In the ideally symmetric mixture, in which the individual properties of polymers A and B are the same and both have the same surface energy, polymers of the minority component segregate to the surface, where they are exposed to less polymers of the majority component. This effect can only be captured correctly, if one accounts for the fact that the monomer-monomer interaction has finite range. As a consequence, the Flory-Huggins-parameter varies in space and depends on the concentration profiles and their derivatives. The surface segregation calculated with such an ansatz, without any fit parameter, is in reasonable quantitative agreement with data from recent Monte Carlo simulations.

1 Introduction

Many important properties of materials are determined by the structure of their surfaces (adhesive properties, thin film properties etc.). Polymeric substances are affected by the presence of a surface on many different length scales: rearrangement of monomers similar to the layering and packing of molecules at surfaces of simple liquids, reorientation of monomers, reorientation of whole chains, surface induced ordering in copolymer systems, wetting and other surface induced transitions[1, 2]. One of the most remarkable effects at surfaces of polymeric mixtures is the phenomenon of surface segregation - the composition of the melt close to the surface differs from that in the bulk. The reasons for such a behavior are manifold. Shorter chains tend to segregate to the surface because they loose the least entropy entropy there[3, 5, 4]; Stiffer chains are favored at the surface because they pack more easily[5]. Hard walls may interact with the different polymer species with different interaction strength. At free surfaces, segregation is induced by "missing neighbor effects": The polymer species with the lower monomer-monomer attraction segregates, since it is less penalized for the lack of neighbors at the surface – it's surface energy is lower[6]. A similar effect occurs even in completely symmetric mixtures of two incompatible, but otherwise "identical" polymers. The minority component enriches at the surface, because it has less contacts with polymers of the majority component there. This interaction driven segregation is a general phenomenon, which is found in many systems with a tendency of bulk ordering (the "ordering" here being the demixing of the two polymer species). It can be expected in the one-phase region as well as in the two-phase region, and is strongest in the vicinity of the critical demixing point[7]. An additional aspect of surface segregation in polymeric systems has to do with the competition of length scales there: the single chain gyration radius competes with the typical length scale for collective concentration fluctuations, which diverges at the critical point.

Experimental studies have mainly been concerned with surface segregation in polymer mixtures in the one-phase region[8]-[11]. Popular systems are, for example, mixtures of polystyrene (PS) and deuterated polystyrene (dPS), or of hydrogenated and deuterated polymethylmethacrylate (PMMA and dPMMA). The surface of PMMA/dPMMA mixtures saturates with dPMMA almost independently of chain lengths and bulk composition[11]. Hence the difference between the surface energies of the components is presumably very high and entirely dominates the segregation process. The segregation tendency of dPS in PS/dPS mixtures is much weaker and the dPS excess at the surface depends strongly on the bulk volume fraction. The relative importance of different segregation mechanisms can be estimated by simple considerations.

The excess surface energy of dPS at vanishing bulk volume fraction is roughly $\mu \approx 2 - 3 \cdot 10^{-3} nm$[9] at temperature $184^0 C$. The Flory Huggins parameter χ, which measures the relative repulsion of monomers of the two components, takes the value $\chi = 1.5 \cdot 10^{-4}$, and the polymer segment length is $a = 0.67nm$. From comparing μ to χa, one concludes that the segregation process is still mainly driven by the excess surface energy, but that interaction driven segregation may become important. An even stronger effect can be expected in mixtures where χ is larger.

Apart from experiments, Computer simulations provide additional understanding and a good testing ground for theories[12]. Monte Carlo simulations of simple one component polymer melts at surfaces have given insight into the structure of polymer chains close to the surface – chain end distributions, chain orientations, etc.[13]-[16]. Being computationally very demanding, simulations of polymer blends at surfaces are still scarce. Wang et al have investigated the wetting behavior of very short chains[17] at walls with very strong attraction of one species. In a recent study, Rouault et al[18] consider incompatible symmetric polymer blends at "neutral" walls and find, as expected, segregation of the minority component there. In contrast, Cifra et al[19] study fully compatible blends, where the missing neighbor effect leads to the enrichment of the majority component at the surface.

Theoretical treatments of polymeric surfaces have often dealt with simple Flory-Huggins-de Gennes functionals of the concentration profiles in "square gradient" approximation[20]-[24]. Jones et al[10, 23] first pointed out that this type of theory fails to reproduce the correct form of segregation profiles: Unlike profiles typically obtained from Ginzburg-Landau theories, experimental profiles are flattened right at the surface. More sophisticated mean field approaches take the chain connectivity into account more explicitly, either in the framework of integral equation theories or density functional theories[25]-[33], or in the self consistent field theory originally developed by Helfand and others[34]-[38], or, lately, in combinations of the two approaches[31, 33]. A recent study by Genzer et al[39] has shown that profiles of polymer blend surfaces calculated within the self consistent field theory can indeed be fitted to experimentally measured profiles in a satisfactory way. However, Genzer et al treat the blend as an incompressible mixture, a simplification which is clearly not justified when treating free surfaces. Surface segregation is enforced by external ad hoc potentials acting on the surface layer. The theory does not allow for a microscopic treatment of missing neighbor effects.

The importance of compressibility effects in polymer melts has been recognized by several authors. In the early work of Helfand et al, they are taken into account within a quadratic approximation. This is reasonable as long

as one deals with small total density fluctuations, not in the vicinity of a surface where the density goes down to zero. Some work has been devoted to elaborated density functional theories of one component polymer melts at surfaces[25, 26, 27, 32]. Those studies have had remarkable success in reproducing the density profiles measured in corresponding Monte Carlo Simulations; however, they mainly focussed on the microscopic structure of a melt over the length scale of the monomer size – here, we are interested in composition variations on a larger scale. Freed and coworkers have developed density functional theories of compressible polymer blends[30]. Recently, Hariharan and Harris have presented a self consistent field study of the surface of a compressible copolymer melt within the framework of the Scheutjens and Fleer lattice theory[37, 40]. Compressibility can be introduced into lattice models in a relatively straightforward way by admitting vacancies as a new type of "particles" which may occupy a lattice site. To the present author's knowledge, no attempt has been made so far to study surfaces of compressible polymer mixtures in continuum space.

This is the scope of the present work. On the base of the equation of state which is assumed to be known and using elements of simple density functional theory, a self consistent field theory for compressible polymer melts will be developed. In self consistent field theory, monomer-monomer interactions are commonly treated as contact interactions $V(\vec{r}) \propto \chi\delta(\vec{r})$. Such a potential Ansatz is not suitable for the description of important missing neighbor effects – e.g. the effect that, close to a hard wall, monomers a $z > 0$ have no neighbors at $z < 0$. Hence the theory will be extended such that it accounts for the finite range of interactions. The parameters of the theory will be adapted to the bond-fluctuation model used in the Monte Carlo simulations of Rouault et al[18].

The bulk properties of the model are very well known from previous work[41, 42]. Müller et al performed large scale simulation studies of interfacial properties in incompatible polymer mixtures[43]. The comparison of his results to self consistent field calculations showed that the theory is rather successful in predicting many quantities even at the relatively short chain length of $N = 32$, except for the interfacial width[45]. The discrepancies between theory and simulation becomes smaller as the chain length is increased, but the convergence is extremely slow. Similarly, we will see here that our self consistent field calculation yield the quantitatively correct values of the surface segregation, without any fit parameter, but fail to predict the correct decay lengths of the profiles.

The paper is organized as follows. The theory is developed and the model parameters are determined in the next section. In section 3, the surface seg-

regation at neutral walls is calculated in the one-phase and in the two-phase region and compared to the available simulation data. The influence of chain length asymmetry on the surface segregation is also studied. Then the structure of the blend at the surface is analyzed in more detail. The evolution of density profiles as one moves away from the critical point will be examined, chain end distributions and chain orientations will be calculated. The results are summarized in section 4.

2 Self consistent field theory for compressible melts

We consider mixtures of flexible polymers A and B in the vicinity of a surface. Each chain of type i ($i = A$ or B) contains N_i monomers and is characterized by a statistical segment length b_i, The radius of gyration of a chain in the homogeneous melt is thus given by ${R_{g,i}}^2 = {b_i}^2 N_i/6$ (random walk). Unless stated otherwise, we will assume that polymers A and B have the same properties, i.e. N, b and the bulk density in a pure system ρ_b are equal for both species.

Molecules are treated as space curves $\vec{r}(s)$, with s varying from 0 to 1. The partition function for a system of n_A polymers of type A and n_B polymers of type B has the general form[35]

$$\mathcal{Z} = \frac{1}{n_A! n_B!} \int \prod_{i=1}^{n_A} \widehat{\mathcal{D}}\{\vec{r}_i(\cdot)\} \prod_{j=1}^{n_B} \widehat{\mathcal{D}}\{\vec{r}_j(\cdot)\} \exp[-\beta \mathcal{F}\{\widehat{\rho}_A, \widehat{\rho}_B\}], \tag{1}$$

where $\beta = 1/k_B T$ is the Boltzmann factor and $\widehat{\rho}_A$, $\widehat{\rho}_B$ are monomer density operators

$$\widehat{\rho}_{A,B}(\vec{r}) = N \sum_{i=1}^{n_{A,B}} \int_0^1 ds\, \delta(\vec{r} - \vec{r}_i(s)) \tag{2}$$

and $\mathcal{F}\{\widehat{\rho}_A, \widehat{\rho}_B\}$ represents a coarse grained free energy functional, which will be discussed in more detail below. Individual space curves in the functional integral are assigned a statistical weight $\widehat{\mathcal{D}}\{\vec{r}(\cdot)\} = \mathcal{D}\{\vec{r}(\cdot)\}\, \mathcal{P}_G\{\vec{r}(\cdot)\}$ with

$$\mathcal{P}_G\{\vec{r}(\cdot)\} = \mathcal{N} \exp[-\frac{3}{2Nb^2} \int_0^1 ds |\frac{d\vec{r}}{ds}|^2], \tag{3}$$

with the normalization factor $\mathcal{N}$. Flexible chains are hence modelled as continuous space curves, which are distributed according to a Gaussian stretching energy with spring constant $3/Nb^2$.

We treat the problem in mean field approximation by replacing the monomer density operator $\widehat{\rho}(\vec{r})$ in eqn (1) with the average monomer density $\rho_i(\vec{r}) := \langle \widehat{\rho}_i(\vec{r}) \rangle$.

Monomer-monomer correlations are ignored. The chains can then be treated as independent random walks in the external field $W_i(\vec{r}) = \frac{\delta(\beta\mathcal{F})}{\delta(\rho_i(\vec{r}))}$ [35]. It is useful to define the end-segment distribution functions

$$Q_i(\vec{r}_0, s) = \int \widehat{\mathcal{D}}\{\vec{r}(\cdot)\} \exp[-\int_0^s ds' W_i(\vec{r}(s'))] \delta(\vec{r}_0 - r(\vec{s})) \tag{4}$$

which obey the diffusion equation[34]

$$\{\frac{1}{N_i}\frac{\partial}{\partial s} - \frac{1}{6}b^2\vec{\nabla}^2_{\vec{r}} + W_i\}\, Q_i(\vec{r}, s) = 0 \tag{5}$$

with initial condition $Q_i(\vec{r}, 0) \equiv 1$. The function Q_i gives the statistical weight for a part of a polymer of type i and length sN, with one end fixed at position $\vec{r}$. The average density of type i monomers (with orientation $\vec{u}$) is then given by

$$\rho_i(\vec{r}) = \rho_b \int_0^1 ds\; Q_i(\vec{r}, s) Q_i(\vec{r}, 1-s), \tag{6}$$

which completes the cycle of self-consistent equations. The calculated profiles can be used to calculate the configurational entropy of a polymer of type i

$$\mathcal{S}_i = k_B(\log \mathcal{Z}_i + \frac{1}{n_i}\int d\vec{r} W_i(\vec{r})\rho_i(\vec{r})), \tag{7}$$

where the single chain partition function $\mathcal{Z}_i = \int d\vec{r} Q_i(\vec{r}, 1) = N n_i/\rho_b$ is a constant. From there one gets the free energy

$$\beta F = \beta\mathcal{F}\{\rho_A, \rho_B\} - \frac{1}{k_B}(n_A\mathcal{S}_A + n_B\mathcal{S}_B). \tag{8}$$

We now turn to the discussion of the free energy functional $\mathcal{F}\{\widehat{\rho}_A, \widehat{\rho}_B\}$, which defines the concrete model. We assume that species dependent interactions between monomers can be treated as perturbations of a reference system "0", in which there is no distinction between monomers of different type.

$$\mathcal{F}\{\rho_A, \rho_B\} = \mathcal{F}_0\{\rho\} + \mathcal{F}_{inter}\{\rho_A, \rho_B\} \qquad \text{with} \qquad \rho = \rho_A + \rho_B \tag{9}$$

More specifically, our Ansatz is based on a reference system of noninteracting polymers with simply hard core repulsion. We can treat the reference system in local density approximation

$$\beta\mathcal{F}_0\{\rho\} = \int d\vec{r}\rho(\vec{r})(f[\rho(\vec{r})] - \mu). \tag{10}$$

The bulk free energy per monomer $f(\rho)$ can be calculated from the equation of state $\Pi(\rho)$ (with the pressure Π) using

$$f(\rho) = \int_0^\rho dx\, \Pi(x)/x^2; \tag{11}$$

the chemical potential μ drives the total number of particles and is related to the bulk density ρ_b via $\mu = f(\rho_b) + \rho_b \frac{\partial f}{\partial \rho_b}$. We will use the equation of state resulting from the generalized Flory theory in continuous space proposed by Dickman and coworkers[46, 47].

$$\Pi = C_0 \rho [\frac{1 + \eta + \eta^2 - \eta^3}{(1-\eta)^3} - 1], \tag{12}$$

for long enough chain lengths. The constant C_0 is $C_0 = 0.6583$, and the "packing fraction" η is given by $\eta = a^3 \rho \pi / 6$ with the "monomer diameter" $a = 1.96 a_0$ in the bond fluctuation model[47] (where a_0 is the lattice spacing). This theory has been remarkably successful in predicting the correct pressures for the athermal bond-fluctuation model over a wide range of densities. At the interesting density $\rho = 1/16 a_0^{-3}$, however, it yields a compressibility $\kappa = 34 a_0^3$ which is slightly too high ($\kappa \approx 31 a_0^3$ according to simulations[42]). In order to correct for this, a higher order term is added to $f(\rho)$,

$$f(\rho) = C_0 \frac{\eta(4 - 3\eta + b\eta^3)}{(1-\eta)^2} \qquad \text{with} \qquad b = 3.0. \tag{13}$$

The ad-hoc correction to the generalized Flory theory ($b = 0$) is motivated by the fact that the equation of state derived from (13), $\Pi = \rho^2 f'(\rho)$, is numerically almost identical with (12) in the relevant density region $0 \leq \rho \leq a_0^3/16$. Calculations have also been performed at $b = 0$ or with a completely different form of $f(\rho)$ (a quadratic expansion around $\rho = a_0^3/16$, cf. [45]) – the results appear to be rather insensitive to details of the equation of state.

The formalism so far takes care only of the hard core repulsion between monomers. In a perturbative treatment, monomers A and B are assumed to interact with each other with additional integrable potentials $U_{AA}(\vec{r})$, $U_{BB}(\vec{R})$ and $U_{AB}(\vec{r})$, and the energetic contribution to the free energy is given by

$$\mathcal{F}_{inter} = \int d\vec{r} d\vec{r}' \frac{1}{2} \Big[\sum_{i,j} \rho_{ij}^{(2)}(\vec{r}, \vec{r}') U_{ij}(\vec{r} - \vec{r}') \Big], \tag{14}$$

where the indices i, j run over the polymer species A and B, and $\rho_{ij}^{(2)}(\vec{r}, \vec{r}')$ is the pair density of type i monomers at point $\vec{r}$ and type j monomers at point $\vec{r}'$. We use the simple approximation

$$\rho_{ij}^{(2)}(\vec{r}, \vec{r}') = \gamma(\vec{r} - \vec{r}') \rho_i(\vec{r}) \rho_j(\vec{r}'), \tag{15}$$

where $\gamma(\vec{r})$ does not depend on densities any more, but does account for local effects of chain connectivity. A possible choice is $\gamma(\vec{r}) = 0$ inside the excluded volume of the central monomer, and $\gamma(\vec{r}) = 1 - p(\vec{r})$ outside, where $p(\vec{r})$ is

the probability that direct neighbor monomers along the chain block point $\vec{r}$ for occupation. The Ansatz (15) is chosen in the usual spirit of Flory Huggins type theories, where monomers are subject to averaged fields created by *all* other monomers, and the effect of long range concentration correlations induced by chain connectivity is ignored. This implies that the demixing behavior is governed by the *inter*chain interactions, as has indeed been found in simulations, see ref. [44]. Hence the pair correlation function $\gamma(\vec{r})$ is taken to be independent of the identity of the monomers. Note that, as soon as intrachain interactions become important, demixing goes along with the collapse of polymers and the Helfand treatment of chains as random walks is no longer appropriate.

Equation (14) can now be rewritten as

$$\beta\mathcal{F}_{inter} = \int d\vec{r}d\vec{r}'\gamma(\vec{r}-\vec{r}')[\rho(\vec{r})\rho(\vec{r}')V_1(\vec{r}-\vec{r}') + \rho_A(\vec{r})\rho_B(\vec{r}')V_2(\vec{r}-\vec{r}') + (\rho_A(\vec{r})-\rho_B(\vec{r}))\rho(\vec{r}')V_3(\vec{r}-\vec{r}')] \tag{16}$$

with

$$\begin{aligned} V_1(\vec{r}) &= \frac{\beta}{4}(U_{AA}(\vec{r}) + U_{BB}(\vec{r})) \\ V_2(\vec{r}) &= \frac{\beta}{2}(2U_{AB}(\vec{r}) - U_{AA}(\vec{r}) - U_{BB}(\vec{r})) \\ V_3(\vec{r}) &= \frac{\beta}{4}(U_{AA}(\vec{r}) - U_{BB}(\vec{r})). \end{aligned}$$

The first term depends only on the total density profile $\rho(\vec{r})$ and does not introduce qualitative changes compared to the reference state $\mathcal{F}_0$. The second term describes effective interactions between monomers A and B, and the third term an effective field favoring one of the components. One can see this from looking at the homogeneous bulk system. For $i = 1, 2, 3$ we define

$$u_{b,i} = \rho_b \int d\vec{r}\gamma(\vec{r})V_i(\vec{r}). \tag{17}$$

The contribution (16) to the bulk free energy is then given by

$$\beta\mathcal{F}_{inter,b} = u_{b,1}n + u_{b,2}n_An_B/n + u_{b,3}(n_A - n_B), \tag{18}$$

with the total number of monomers n_A, n_B and $n = n_A + n_B$. Hence we can identify $u_{b,2}$ with the Flory Huggins parameter χ_b, and $u_{b,3}$ with an effective chemical potential difference h_b.

We assume that the potentials U_{ij} are short range and expand the profiles $\rho_{A,B}(\vec{r}')$ around $\vec{r}$. Since we study a planar surface, the system is inhomogeneous only in one space variable z. Using $\int d\vec{r}\gamma(\vec{r})V_i(\vec{r})z = 0$ (due to the

inversion symmetry of V and γ), and defining

$$k_i = \frac{\rho_b}{2u_{b,i}} \int d\vec{r}\gamma(\vec{r})V_i(\vec{r})z^2, \tag{19}$$

one can reexpress terms of the form $\int d\vec{r}d\vec{r}'\rho_\alpha(\vec{r})\rho_\beta(\vec{r}')V_i(\vec{r}-\vec{r}')\gamma(\vec{r}-\vec{r}')$ by $\int dz\rho_\alpha(z)(\rho_\beta(z)+\rho''_\beta(z)k_i)u_{b,i}/\rho_b$, where $\alpha,\beta = A$ or B. One obtains the total free energy[49]

$$\begin{aligned}\beta\mathcal{F} &= \int dz\{\rho(z)(f[\rho(z)]-\mu)+\frac{u_{b,1}}{\rho_b}\rho(z)(\rho(z)+k_1\rho''(z)) \\ &\quad +\chi(z)\rho_A(z)\rho_B(z)/\rho_b + h(z)(\rho_A(z)-\rho_B(z))\}\end{aligned} \tag{20}$$

with the space dependent Flory-Huggins parameter $\chi(z) = \chi_b(1+\frac{1}{2}k_2(\frac{\rho''_A}{\rho_A}+\frac{\rho''_B}{\rho_B}))$ and the space dependent field $h(z) = h_b(\rho+k_3\rho'')/\rho_b$. The difference to the bulk values of χ and h reflects the missing neighbor effects and is ultimately responsible for the occurrence of segregation. This is obvious for the field $h(z)$ – as we will see, it is also true for $\chi(z)$. From eqn (20) one can calculate the mean fields

$$\begin{aligned}W_A(z) &= \zeta(z)+\chi_b(\rho_B+k_2\rho''_B)/\rho_b + h(z) \\ W_B(z) &= \zeta(z)+\chi_b(\rho_A+k_2\rho''_A)/\rho_b - h(z)\end{aligned} \tag{21}$$

with

$$\zeta(z) \approx \rho\frac{df}{d\rho} + f(\rho) - \mu + \zeta_{inter}(z), \tag{22}$$

$$\zeta_{inter}(z) = 2(\rho+k_1\rho'')\frac{u_{b,1}}{\rho_b} + ((\rho_A-\rho_B)+k_3(\rho''_A-\rho''_B))\frac{h_b}{\rho_b}$$

We will assume that the perturbation $\mathcal{F}_{inter}$ is small compared to $\mathcal{F}_0$ and that the corresponding contributions to $\zeta(z)$, $\zeta_{inter}(z)$, can be neglected.

To summarize, elements of a simple classical density functional theory (the local density approximation for the treatment of hard core monomer interactions in connection with perturbative treatment of attractive interactions) have been introduced into the Helfand formalism, in order to enable the study of compressible systems with intermonomeric interactions of finite range. A similar approach has been taken by S.K. Nath et al in order to study surfaces of homopolymer melts[33]. We note that it has some inconsistencies, polymers are treated as gaussian strings, whereas monomers are assumed to have finite size. This should however be of little importance, as long as we are interested in density variations on scales larger than the monomer size, and as long as the chains are much longer than the monomers.

The model parameters are adjusted to fit the bond fluctuation model, with the model parameters used by Rouault et al in their Monte Carlo simulation[18]. The bond fluctuation model is a lattice model, where monomers occupy each a cube of eight neighboring sites and are connected by bond vectors of length $2 \leq d \leq \sqrt{10}$ lattice spacings. Thus the excluded volume of a monomer is $V_{excl} = 27a_0^3$. Simulations are often carried out at monomer density $\rho = 1/16a_0^{-3}$, where one half of all available lattice sites are occupied and the model reproduces many properties of dense polymer melts. Rouault et al simulated polymers of length 32 and used the interaction potentials $U_{AA}(\vec{r}) = U_{BB}(\vec{r}) = -U_{AB}(\vec{r}) = -k_BT\epsilon$ for $|\vec{r}| \leq \sqrt{6}$, i.e. they have $V_1 = -\epsilon/2$, $V_2 = 2\epsilon$ and $V_3 = 0$ within the interaction range. No effective field $h(z)$ is induced, since the interaction parameters are symmetric with respect to A and B. The sites in the interaction region $2 \leq |\vec{r}| \leq \sqrt{6}$ of a monomer are at the relative positions $\vec{r} = (200), (210), (211)$, plus permutations of the coordinate axes and sign reversals. Hence the interaction region covers $N_t = 54$ sites, $N_2 = 18$ of which are located at distances $z = \pm 2$ from the central site along the z-direction, and $N_1 = 24$ at distances $z = \pm 1$. Assuming that a site in the interaction range of a monomer is blocked by one of its neighbor monomers along the chain with the probability $p = 1/3$, a rough estimate of the function $\gamma(\vec{r})$ yields $\gamma(\vec{r}) = 1 - p = 2/3$ in the interaction region and therefore $\chi_b = V_2 z_{eff}$ with the effective coordination number $z_{eff} = (1-p)N_t\rho_b$ with $\rho_b = 1/16$ (cf. eqn.(17)). The value $z_{eff} = 2.25$ calculated from this approximation is reasonably close to the average number of interchain contacts found in simulations, $z_{eff} = 2.65$ at chain length 32[43]. Similarly, one estimates from eqn (17) and eqn(19) $k_2 = \sum_j j^2 N_j/(2N_t) = 8/9$.

It should be emphasized that the theory was adjusted to the bond fluctuation model, a lattice model, for the sole reason that simulation data are available, which permit to test the theoretical predictions. Adjusting the theory to continuous off-lattice models causes no conceptual difficulties in most cases. It requires the knowledge of the equation of state in a reference system of identical polymers, a reasonable guess of the pair correlation function $\gamma(\vec{r})$, and the knowledge or a good ansatz for additional integrable intermonomeric interactions U_{AA}, U_{AB} and U_{BB}, which are small enough to be treated perturbatively. Extensions of the theory will be necessary if the origin of the Flory-Huggins parameter χ is mostly entropic, e.g. if polymers A and B demix as a result of different monomer sizes.

A surface at $z = 0$ is imposed by requiring $\rho_i(z) \equiv 0$ for $z < 0$; at the bulk side, the boundary conditions $\frac{\partial}{\partial y} Q_i(z_{max}, s) = 0$ and $W_i(z_{max}) = W_{i,bulk}$ were used, where $W_{i,bulk}$ denotes the bulk value of the fields W_i. The numerical method used to find the self consistent solution of the diffusion equation was

an iterative relaxation technique described in ref. [45]. The iteration cycle was stopped after reaching an accuracy $\Gamma = \sum_i \int dy (\Delta W_i)^2$ of 10^{-14}. (relative accuracy $\geq 10^{-15}$).

3 Results

The system shows the usual bulk demixing phase behavior. From eqns (5) and (6), one can see that the bulk volume fractions $\Phi_{A,B} = \rho_{A,B}/\rho_b$ obey the mean field equations $\Phi_i = \exp(-N_i W_i)$ or, equivalently, $\partial F/\partial \rho_i = \log(\Phi_i)/N_i + W_i = 0$ with the Flory type bulk free energy per volume

$$\beta F = (\rho_A + \rho_B) f(\rho_A + \rho_B) + \sum_i \frac{\rho_i}{N_i} \log(\Phi_i) + \frac{\chi_b}{\rho_b} \rho_A \rho_B - \sum_i H_i \rho_i, \qquad (23)$$

and $H_A = \mu + h_b + 1/N_A, H_B = \mu - h_b + 1/N_B$. It is useful to rewrite the free energy as a function of the total density $\rho = \rho_A + \rho_B$ and the density difference $m = \rho_A - \rho_B$. A homogeneous blend is stable or metastable with respect to small fluctuations in m as long as $[\partial^2 F/(\partial m)^2]_\rho = (\chi_s - \chi)/(2\rho_b) > 0$ with the spinodal $\chi_s = (1/(N_A \Phi_A) + 1/(N_B \Phi_B))/2$. The spinodal ends in the critical point, which is characterized by $[\partial^2 F/(\partial m)^2]_\rho = 0$ and $[\partial^3 F/(\partial m)^3]_\rho = ((1/(N_A \Phi_A^2) - 1/(N_B \Phi_B^2))/(2\rho_b) = 0$. Hence one gets the critical χ parameter and critical volume fractions

$$\Phi_{A,c} = \frac{\sqrt{N_B}}{\sqrt{N_A} + \sqrt{N_B}} \qquad \Phi_{B,c} = \frac{\sqrt{N_A}}{\sqrt{N_A} + \sqrt{N_B}} \qquad \chi_c = \frac{1}{2} \left(\frac{1}{\sqrt{N_A}} + \frac{1}{\sqrt{N_B}} \right)^2 \qquad (24)$$

At low temperatures or $\chi > \chi_c$, the mean field equations have no stable homogeneous solution for a range of concentration differences m, i.e. the system demixes. This implies that there exist two distinct solutions in a range of h_b, one finds metastable states or two phase coexistence; at χ_c the two solutions merge continuously into one. The order parameter of the system can be defined as the difference of volume fractions in the two coexisting phases. In the symmetric system with equal chain lengths $N_A = N_B$, two-phase coexistence occurs below the critical point $(\chi N)_c = 2$ at $h_b = 0$ (see Fig. 1).

3.1 Surface segregation

Figure 2 shows a segregation profile in a symmetric mixture at bulk two phase coexistence. The volume fraction of the minority component is increased almost by a factor of two at the surface. After a flatter part, the composition

profile decays towards the bulk value within $2-3$ times the gyration radius R_g. The total density profile is shown in the inset: The density reaches the bulk value much more quickly than the composition profile. This reflects the different length scales involved in the problem: The relaxation of the total density profile involves rearrangement of single "monomers", it is hence driven by the Kuhn length b. The composition change at the surface, on the other hand, goes along with the segregation of whole chains – the thickness of the segregation layer has to be of the order of at least the gyration radius R_g. The fine structure of the profiles will be discussed in more detail later. It is worth noting that the extent of surface segregation strongly depends on the range of the monomer interactions or the value of k_2. In the limit of $k_2 = 0$ or pure contact interactions, segregation is almost entirely suppressed (dashed line).

Apart from the bulk phase diagram, Figure 1 also indicates the surface volume fraction of component A in the different phases as a function of "temperature" $1/\chi N$ at two-phase coexistence. The difference $\Delta\Phi_A$ between surface and bulk volume fraction predicted by the theory is compared to the simulation results of Rouault et al in Fig. 3. (Note that our mean field theory overestimates the critical temperature and does not describe correctly the Ising-type critical behavior found in short chain systems[41, 43], but the region near criticality is not our main interest here.) The simulations were performed in a slab geometry with a slab thickness of around three times the gyration radius. In such a thin film, the critical temperature is reduced, and so is the order parameter in the two phase region. The difference between the surface volume fraction of the minority phase in the thin film and the bulk volume fraction in an "infinite" system can hence be taken as an upper bound for $\Delta\Phi_A$. A lower bound is given by the difference between the volume fraction at the surface and the center of the film. Figure 3 demonstrates that the theoretical results for $\Delta\Phi_A$ lie nicely within the bounds provided by the simulation data. However, quantitative agreement is only reached if the range of monomer interactions has been accounted for correctly, i.e. k_2 may not be neglected.

The total amount of A segregated at the surface is given by the total excess $Z_A^* = \int dz \rho(z)(\Phi_A(z) - \Phi_{A,b})$. As shown in Figure 4, it can be described by a simple Boltzmann dependence

$$Z_A^* \propto \exp(-\chi N \alpha) \tag{25}$$

over a wide range of χN. In this regime, one can describe the segregation process as adsorption of single, relatively undistorted A chains whose energy is reduced by $\chi N(1-\alpha)$ at the surface, compared to the bulk. The quantity $(1-\alpha)$ thus gives the quota of neighbor monomers, which a chain is missing at the surface. In the present model, one obtains $\alpha = 0.77$. Close to the critical point, interactions between different A chains at the surface become

important and our simple picture breaks down - the surface excess diverges. At very high values of χN, beyond $\chi N \gtrsim 14$, the chains are more and more squeezed at the surface, the number of missing neighbors increases, and the segregation is slightly higher than eqn (25) would predict.

The surface segregation in the one phase region is shown in Figure 5, as a function of bulk volume fraction $\Phi_{A,b}$ at fixed Flory Huggins parameter χ. For comparison, segregation profiles for mixtures of polymers with different chain lengths ($N_B = 2N_A = 48$ or $N_A = 2N_B = 48$ as opposed to $N_B = N_A = 32$) were also calculated. In such asymmetric mixtures, shorter chains segregate to the surface when there are no interactions, at $\chi = 0$, for entropic reasons (thin line). At $\chi \lesssim \chi_c$, however, the segregation is mainly driven by energetic effects: As the bulk volume fraction Φ_A approaches zero, polymers A segregate to the surface to the same extent regardless of whether they have longer or shorter chain lengths than polymers B. The effects of segregation due to a difference in chain lengths, and segregation due to missing neighbor effects, are therefore *not* additive. This becomes most obvious when looking at the surface excess of component A (Figure 5b). On increasing the fraction of chain lengths N_A/N_B while keeping $\chi_c = (1/\sqrt{N_A}+1/\sqrt{N_B})^2/2$ approximately constant, the critical point moves towards the A-poor region of the phase diagram (cf eqn (24)). As a consequence, the excess of A-polymers at the surface is even higher for $N_A > N_B$ than for $N_B > N_A$. Hence the entropic mechanism which promotes segregation of the shorter chains is largely suppressed – the dominant effect of chain length asymmetry is the shift of the critical point.

3.2 Structure of the Profiles

We turn to analyze the segregation profiles in more detail. Far from the critical point, they can be expected to reflect single chain behavior. Figure 4 suggests that one may be able to describe a segregation profile in terms of a weakly adsorbed layer of the minority component. In order to test this picture, we calculate for comparison the density profile of a single Gaussian polymer in semi-infinite space, which touches the surface at least once. This can be done analytically, as shown in the appendix. Far from the surface, the density profile decays asymptotically like $\rho(z) \propto 1/z^3 \exp(-z^2/(4R_g^2))$. The logarithmic derivative is thus given by

$$R_g \frac{d \log \rho(z)}{dz} = -\frac{3R_g}{z} - \frac{z}{2R_g}. \tag{26}$$

Figure 6 shows the logarithmic derivative of segregation profiles $\rho_A(z)$ in the two-phase region at different values of χ, compared to the prediction of eqn

(26) (dashed line). Far from the critical point, our simple picture describes the asymptotic behavior surprisingly well. Close to the critical point, the logarithmic derivative of $\rho_A(z)$ approaches a constant at large z: The segregation profile decays exponentially with a decay length ξ. This is characteristic for a system close to a critical point. The interactions between chains become important, and collective effects determine the structure of the profiles. In polymeric systems, the characteristic length scale ξ for collective concentration fluctuations competes with the gyration radius R_g, which describes the correlations produced by chain connectivity – the correlations of monomers belonging to the same chain. The result is a crossover between two types of qualitatively different asymptotic behavior: Far from the critical point, intrachain correlations dominate, close by, collective concentration correlations do. The correlation length ξ diverges at the critical point.

We can again attempt to compare these results with the simulations of Ref. [18]. Simulations where performed at values $\chi N = 3 - 4$, where the asymptotic behavior of the profiles is still governed by the length scale ξ. At film thicknesses of less than $3R_g$, however, the asymptotic behavior is never reached. This may explain why the decay length obtained by Rouault et al, $\xi \approx 0.35R_g$ at $\chi N = 3.4$, is only roughly half the value predicted by the self consistent field theory, $\xi \approx 0.6R_g$.

The decay length ξ as a function of $1/\chi N$ is shown in Figure 7, and compared to half the width of the bulk interface between the two coexisting phases, which has been calculated in Ref. [45]. In a simple system, both lengths are identical, i.e. by the bulk correlation length. Here, this is only true very close to the critical point; further away, ξ gets too large relative to the interfacial width. This is due to the fact that the wings of the segregation profiles are governed by the chain end distribution, as we shall see in the next section. The interfacial width, on the other hand, describes the separation of all A and B monomers. Chain end distributions tend to be broader than total monomer distributions for entropic reasons. In the wings of the interfacial profile, we expect to find a decay length which is again determined by the chain end distributions and identical to ξ. This is indeed the case (not shown).

Figure 7 also shows data for another length which characterizes the segregation profiles, the profile width. It is conveniently defined through the excess distribution $Z_A(z) = \rho(z)(\Phi_A(z) - \Phi_{A,b})/\rho_b$, e.g. as its first moment or as its standard deviation.

$$W_{\langle z\rangle} = \frac{\int dz\, zZ_A(z)}{Z_A^*} \qquad W_{\langle \delta z^2\rangle} = \sqrt{\frac{\int dz\, z^2 Z_A(z)}{Z_A^*} - (\frac{\int dz\, zZ_A(z)}{Z_A^*})^2} \qquad (27)$$

At the critical point, the width diverges with the correlation length ξ. Further

away, it reaches a plateau at $W \approx R_g/\sqrt{3}$, which is about the extention of an undistorted chain in one dimension. At large values of χN, however, the width decreases further and approaches zero. The strong repulsion between chains A and B cause the segregated chains to get increasingly distorted and squeezed towards the surface. The turning point of the curve is at $1/\chi N \approx 0.07$ or $\chi N \approx 14$, consistent with what was already deduced from the χN–dependence of the surface excess Z_A^* in Figure 4.

3.3 Chain end distributions and Chain orientations

Figure 8 compares the distribution of chain ends with density profiles close to the surface at bulk two phase coexistence. For both the minority and the majority component, the fraction of chain ends relative to the total density is augmented right at the surface, and reduced in a region underneath. Such an effect is already known from pure systems[14, 16]. In the minority component, the depletion zone is followed by another enrichment zone in the wings of the decaying segregation profile – polymers of the minority component rather stick out chain ends into the majority phase than whole loops. Thus the segregated layer of polymers A is skirted by regions of enhancement of chain ends A. The total chain end distribution profile, however, only has one enrichment zone right at the surface. One can probably expect a second zone at higher segregation, beyond the wetting transition, since chain ends are known to enrich at the A/B interface [43, 45]. In our simple picture of an adsorbed polymer layer, the chain end distribution decays asymptotically like $\rho(z) \propto 1/z \, \exp(-z^2/(4R_g^2))$ (see appendix), i.e. the logarithmic derivative follows

$$R_g \frac{d \log \rho_{end}(z)}{dz} = -\frac{R_g}{z} - \frac{z}{2R_g}. \tag{28}$$

This is compared to the logarithmic derivative of chain end distributions of the segregating component at different values of χ in Figure 9. The agreement for high values of χN is not as good as for the total density profiles, but still remarkable. Close to the critical point, the profiles show asymptotically again exponential decay with the decay length ξ.

The orientation of whole chains can be studied by solving the diffusion equation (5) in the previously determined self consistent field W_i with initial condition $Q_i(\vec{r}, 0) = \delta(\vec{r} - \vec{r}_0)$. The statistical weight of a polymer with end-to-end vector $\vec{R}_e = \vec{r}_1 - \vec{r}_0$ and center at $\vec{R}_c = (\vec{r}_1 + \vec{r}_0)/2$ is then given by $Q_i(\vec{r}_1, 0)$. Since the self consistent field W_i only varies in the direction perpendicular to the interface, z, the components of the end-to-end vector parallel to the interface have the same distribution at the surface than in the bulk. The

presence of a surface only affects the z-component $R_{z,e}$. Chains get therefore oriented as a result of stretching or squashing in the z direction, the theory does not allow for the possibility of chain orientation without compression, as has been observed in computer simulations[14]. Profiles of $\langle {R_{e,z}}^2 \rangle(z)$, where the averages have been performed for polymers with center at z, are shown in Figure 10. The bulk value of this quantity is simply $2{R_g}^2$ with the gyration radius R_g. Near the surface, it is greatly reduced – it drops down to zero at $z = 0$ and remains smaller than the bulk value over a distance of more than one gyration radius from the surface. Hence polymers tend to align parallel to the surface. This region is followed by a zone of perpendicular alignment at the distance $2R_g$ from the surface (Figure 10). Both the parallel alignment[15] and the subsequent "overshoot" of perpendicular alignment[16] have been seen in Monte Carlo simulations of on one component polymer melts. The latter effect is weak for chains of the majority component, but can be quite marked for the minority component, deep in the two-phase region. The extent of parallel alignment, on the other hand, does not depend on whether a chain belongs to the minority or the majority component, or on the strength of the interaction χ. Thus we find that the total structure of the blend does not change with increasing χ, although the segregated minority component chains get more and more distorted, as indicated by Fig. 7. They just accumulate closer to the surface, where the distortion is higher.

4 Summary

A self consistent field theory for compressible binary polymer mixtures has been developed, which allows for a consistent treatment of surfaces, including effects of missing neighbors. It has been shown to be remarkably successful in reproducing Monte Carlo results for the segregation at a neutral surface in the bulk coexistence region, without resorting to any fitting parameter. On this base, several aspects of the surface structure could be discussed, like the role of chain end distribution and chain orientations, the effect of chain length asymmetry, and the interplay of the different length scales which govern the system: the correlation length of collective concentration fluctuations and the single chain correlation length, i.e. the gyration radius. Hence we have seen that the formalism developed in this work is suited for the investigation of surfaces of polymer mixtures. So far it has only been applied to systems with perfectly symmetric interactions (where $V_3(\vec{r}) \propto (U_{AA}(\vec{r}) - U_{BB}(\vec{r}))$ (eqn (16)) vanishes), a rather unlikely situation in real systems. Usually the asymmetry of the interactions introduces additional surface potentials $h(z)$ (cf. eqn (21), i.e.

preferential attraction of one component to the surface, After taking those into account, the theory should be similarly successful in describing experimental results.

I wish to thank K. Binder for suggesting the problem and for useful comments on the manuscript, and L. Klushin and O. Borisov for helpful discussions.

Appendix

We consider a Gaussian Polymer of length N in the half space with end monomers located at distances z_0 and z_1 from the surface, which touches the surface with the Kth monomer (Figure 11). The Greens function for propagation in the half space can be obtained with the method of mirror images

$$G(M,z;M',z') \propto \exp(-\frac{(z-z')^2}{\frac{2}{3}(M'-M)b^2}) - \exp(-\frac{(z+z')^2}{\frac{2}{3}(M'-M)b^2}), \tag{29}$$

where b is the Kuhn length, and z, z' are the locations of monomer M and M' [48]. Hence the distribution profile of monomer L is given by

$$D_L(z|0,z_0;K,\epsilon\to 0^+;N,z_1) \propto \tag{30}$$

$$\lim_{\epsilon\to 0^+} \begin{cases} G(0,z_0;L,z)G(L,z;K,\epsilon)G(K,\epsilon;N,z_1) & : \quad K>L \\ G(0,z_0;K,\epsilon)G(K,\epsilon;L,z)G(L,z;N,z_1) & : \quad L>K \end{cases}.$$

In order to get the total density of the Lth monomer, one has to integrate over the free parameters z_0, z_1 and K. The result is

$$\rho_L(z) \propto g_l(\alpha z)\sqrt{l}\sqrt{1-l} \tag{31}$$

with

$$g_l(x) = -x\Big[\Phi(\frac{x}{\sqrt{l}})\mathrm{Ei}(-\frac{x^2}{1-l})\frac{1}{\sqrt{1-l}} + \Phi(\frac{x}{\sqrt{1-l}})\mathrm{Ei}(-\frac{x^2}{l})\frac{1}{\sqrt{l}}\Big],$$

where $l = L/N$ and $\alpha = 1/(2R_g)$ with the gyration radius $R_g^2 = Nb^2/6$. The error function Φ is defined as $\Phi(x) = \frac{2}{\sqrt{\pi}}\int_0^x \exp(-t^2)\,dt$, and the exponential integral Ei as $-\mathrm{Ei}(-x) = \int_x^\infty \exp(-t)/t\,dt$. Note that the normalization factor $\mathcal{N}(\sqrt{l}) = \int_0^\infty dx g_l(x)$ is finite and nonzero for all values of l between zero and one. The total density profile is given by

$$\rho(z) = \int_0^1 dl\; g_l(\alpha z)/\mathcal{N}(\sqrt{l}). \tag{32}$$

The asymptotic behavior of the profiles can be obtained from the asymptotic behavior of $g_l(x)$:

$$g_l(x) \stackrel{x\to\infty}{\longrightarrow} \frac{1}{x}[\,\exp(-\frac{x^2}{1-l})\sqrt{1-l} + \exp(-\frac{x^2}{l})\sqrt{l}\,]. \tag{33}$$

The result for the chain end distribution follows immediately.

$$\rho_0(z) = \rho_1(z) \propto \frac{1}{z}\exp(-(\alpha z)^2) \tag{34}$$

The asymptotic behavior of $\rho(z)$ is slightly more difficult to derive. Wihout calculating $\mathcal{N}^{-1}(y)$ explicitly, we expand it in powers of y: $\mathcal{N}^{-1}(y) = \sum_k c_k y^k$. Using asymptotic series representations of the error function and the exponential integral, one can show

$$\int_0^1 dl\, l^{k/2} e^{-x^2/l} \stackrel{x\to\infty}{\longrightarrow} e^{-x^2}\frac{1}{x^2}\sum_{j=0}^{N}(-1)^j\frac{\Gamma(j+k/2)}{\Gamma(k/2)}(\frac{1}{x^2})^j + \mathcal{R}_N, \tag{35}$$

with the Gamma function Γ and $\mathcal{R}_N < x^{-2(N+1)}\Gamma(N)$. With that one obtains

$$\begin{aligned}
\rho(z) &\approx \frac{2}{\alpha z}\sum_{k=0}^{\infty} c_k \int_0^1 dl\, k^{(k+1)/2} e^{-(\alpha z)^2/l} \\
&\approx \frac{2}{(\alpha z)^3} e^{-(\alpha z)^2}\sum_{k=0}^{\infty} c_k \sum_{j=0}^{N}(-1)^j\frac{\Gamma(j+(k+1)/2)}{\Gamma((k+1)/2)}(\frac{1}{x^2})^j \\
&\longrightarrow 2c_0 e^{-(\alpha z)^2}\frac{1}{(\alpha z)^3}
\end{aligned} \tag{36}$$

References

[1] *Physics of Polymer Surfaces and Interfaces*, Sanchez, I. C. edt., Butterworth-Heinemann, Boston, (1992).

[2] K. Binder, Acta Polymer **46**, 406 (1995).

[3] G.H. Fredrickson, J.P. Donley, J. Chem. Phys. **97**, 8941 (1992).

[4] A. Hariharan, S.K. Kumar, T.P. Russell, Macromolecules **23**, 3584 (1990).

[5] M.A. Carignano, I. Szleifer, Europhysics Lett. **30**, 525 (1995).

[6] A. Hariharan, S.K. Kumar, T.P. Russell, Macromolecules **24**, 4909 (1991).

[7] for reviews, see K. Binder in *Phase Transitions and Critical Phenomena*, Vol. 8, p. 1 (1983), C. Domb and J.L. Lebowitz eds., Academic Press, London; S. Dietrich, ibid, Vol. 12, p.1. (1988).

[8] J. Sokolov *et al.*, Appl. Phys. Lett. **54**, 590 (1989); R.J. Composto *et al.*, Physica B **156**, 434 (1989); T. Mansfield *et al.*, Physica B **173**, 207 (1991); A. Hariharan *et al.*, J. Chem. Phys. **99**, 656 (1993).

[9] R.A.L. Jones *et al.*, Phys. Rev. Lett. **62**, 280 (1988).

[10] R.A.L. Jones *et al.* Europhysics Lett. **12**, 41 (1990); X. Zhao *et al.*, Macromolecules **24**, 5991 (1991); E.J. Kramer, Faraday Discussions **98**, 329 (1994).

[11] S. Tasaki, H. Yamaoka, F. Yoshida, Physica B **180**, 480 (1992).

[12] see ,e.g. *Monte Carlo and Molecular Dynamics Simulations in Polymer Science*, K. Binder edt., Oxford University Press (1995).

[13] R. Dickman, C.K. Hall, J. Chem. Phys. **89**, 3168 (1988).

[14] S. K. Kumar, M. Vacatello, D.Y. Yoon, J. Chem. Phys. **89**, 5206 (1988); Macromolecules **23**, 2189 (1990).

[15] A. Yethiraj, C.K. Hall, J. Chem. Phys. **91**, 4827 (1989); Macromolecules **23**, 1865 (1990); ibid. **24**, 709 (1991); A. Yethiraj, J. Chem. Phys. **101**, 2489 (1994); Phys. Rev. Lett. **74**, 2018 (1995).

[16] J.-S. Wang, K. Binder, J. Phys. I France **1**, 1583 (1991).

[17] J.-S. Wang, K. Binder, J. Chem. Phys. **94**, 8537 (1991); Macrom. Chm., Theory Simul. **1**, 49 (1992).

[18] Y. Rouault, B. Dünweg, J. Baschnagel, K. Binder, Polymer, in press.

[19] P. Cifra, F.E. Karasz, W.J. MacKnight, Macromolecules **25**, 4895 (1992).

[20] H. Nakanishi, P. Pincus, J. Chem. Phys. **79**, 997 (1983).

[21] I. Schmidt, K. Binder, J. Physique **46**, 1631 (1985).

[22] S.M. Cohen, M. Muthukumar, J. Chem. Phys. **90**, 5749 (1989).

[23] R.A.L. Jones, Phys. Rev. E **47**, 1437 (1993).

[24] T. Flebbe, B. Dünweg, K. Binder, J. de Physique **I**, submitted.

[25] C.E. Woodward, J. Chem. Phys. **94**, 3183 (1990); ibid. **97**, 695 (1992); 4527 (1992); C.E. Woodward, A. Yethiraj, J. Chem. Phys. **100**, 3181 (1993).

[26] E. Kierlik, M.L. Rosinberg, J. Chem. Phys. **100**, 1716 (1993).

[27] W.E. McMullen, M. Trache, J. Chem. Phys. **102**, 1449 (1994).

[28] P.-G. de Gennes, J. Chem. Phys. **72**, 4756 (1980); R-J. Roe, Macromolecules **19**, 728 (1986).

[29] H. Tang, K.F. Freed, J. Chem. Phys. **94**, 6307 (1991).

[30] J. Dudowicz, K.F. Freed, Macromolecules **23**, 1519 (1990); M. Lifschitz, K.F. Freed, J. Chem. Phys. **98**, 8994 (1993).

[31] K.F. Freed, J. Chem. Phys. **103**, 3230 (1995).

[32] S. Sen, J.M. Cohen, J.D. McCoy, J.G. Curro, J. Chem. Phys. **101**, 9010 (1994); S. Sen, J.D. McCoy, S.K. Nath, J.P. Donley, J.G. Curro, J. Chem. Phys. **102**, 3431 (1994).

[33] S.K. Nath, J.D. McCoy, J.P. Donley, J.G. Curro, J. Chem. Phys. **103**, 1635 (1995).

[34] E. Helfand, Y. Tagami, J. Polym. Sci. B **9**, 741 (1971); J. Chem. Phys. **56**, 3592 (1971); ibid. **57**, 1812 (1972); E. Helfand, A.M. Sapse, J. Chem. Phys. **62**, 1327 (1975).

[35] E. Helfand, J. Chem. Phys. **62**, 999 (1975).

[36] K.M. Hong, J. Noolandi, Macromolecules **14**, 727 (1981); M.W. Matsen, M. Schick, Phys. Rev. Lett. **72**, 2660 (1994).

[37] J.M.H.M. Scheutjens, G.J. Fleer, J. Chem. Phys. **83**, 1619 (1979).

[38] K.R. Shull, E.J. Kramer, Macromolecules **23**, 4769 (1990); K.R. Shull, Macromolecules **25**, 2122 (1991); ibid. **26**, 2346 (1993); K.R. Shull, A.M. Mayes, T.P. Russell, Macromolecules **26**, 3929 (1993).

[39] J. Genzer, A. Faldi, R.J. Composto, Phys. Rev. E **50**, 2373 (1994).

[40] A. Hariharan, J.G. Harris, J. Chem. Phys. **101**, 3353 (1994).

[41] I. Carmesin, K. Kremer, Macromolecules **21**, 2819 (1988); W. Paul, K. Binder, D.W. Heermann, K. Kremer, J. Physique II **1**, 37 (1991); H.-P. Deutsch, K. Binder, Macromolecules **25**, 6214 (1992).

[42] M. Müller, W. Paul, J. Chem. Phys. **100**, 719 (1993).

[43] M. Müller, K. Binder, W. Oed, J. Chem. Soc. Faraday Trans. **91**, 2369 (1995).

[44] M. Müller, K. Binder, Macromolecules **28**, 1825 (1995).

[45] F. Schmid, M. Müller, Macromolecules **28**, 8639 (1995).

[46] R. Dickman, C.K. Hall, J. Chem. Phys. **85**, 4108 (1986).

[47] H.-P. Deutsch, R. Dickman, J. Chem. Phys. **93**, 8983 (1990).

[48] F.W. Wiegel, *Introduction to Path-Integral Methods in Physics and Polymer Science*, World Scientific, Singapore (1986).

[49] Note that this procedure is not unambiguuous, since α and β can be interchanged. Hence there is some arbitrariness in the exact expression for the total free energy, eqn. (20). This is however not a problem, since the expressions for the mean fields, eqn. (21), remain unequivocal.

Figure Captions

Figure 1: Mean field phase diagram of the symmetric polymer blend with $N_A = N_B = N$ in the plane of variables $1/(\chi N)$ and the volume fraction Φ_A of A monomers. Inside the binodal curve (solid line), the mixture phase separates into two macroscopic phases (1) (left) and (2) (right). Also shown is the surface volume fraction of A monomers at a free surface $\Phi_{1,A}$ in each of the two coexisting phases. Near the critical point, the concentration differences $(\Phi_A^{(1)} - \Phi_A^{(2)})$ and $(\Phi_{A,1}^{(1)} - \Phi_{A,1}^{(2)})$ vanish with different critical exponents: $(\Phi_A^{(1)} - \Phi_A^{(2)}) \propto (\chi_c - \chi)^{\beta}$ with $\beta = 1/2$ and $(\Phi_{A,1}^{(1)} - \Phi_{A,1}^{(2)}) \propto (\chi_c - \chi)^{\beta_1}$ with $\beta_1 = 1$ in mean field theory. Thus the broken curves have a cusp at the critical point.

Figure 2: Volume fraction profile of the minority component monomers at $\chi/\chi_c = 1.696$ in the symmetric polymer mixture. Dashed line shows volume fraction profile for $k_2 = 0$, where monomers are assumed to have pure contact interactions with each other. Inset shows the total density profile, which was identical for all considered values of χ.

Figure 3: Difference $\Delta\Phi_A$ between surface and bulk volume fraction of the minority component monomers in the symmetric polymer mixture, at two phase coexistence, vs. $1/(\chi N)$. Data points show results of the simulations of Rouault et al ([18]): The difference between surface and bulk volume fraction (circles), and the difference between the surface volume fraction and the volume fraction at the center of simulated slab (squares). The arrow indicates the value of $1/(\chi N)$ corresponding to the profiles in Figs 2 and 8.

Figure 4: Surface excess Z_A^* of the minority component at two phase coexistence in the symmetric polymer mixture, in units of $\rho_b R_g$, vs χN. dashed line shows the function $0.3\exp(-0.77\chi N)$.

Figure 5: (a) Difference $\Delta\Phi_A$ between surface and bulk volume fraction of A monomers and (b) surface excess Z_A^* in units of $\rho_b R_g$, in the one phase region, as a function of the bulk volume fraction Considered are symmetric mixtures with $N_A = N_B$ (thick solid line) and asymmetric mixtures, where A polymer chains are either longer (long dashed line) or shorter (short dashed line) than B polymer chains. Thin line indicates results for asymmetric mixtures with the interactions turned out or $\chi = 0$.

Figure 6: Logarithmic derivative of density profiles for the minority component in the symmetrical mixture, in units of R_g^{-1}, at two phase coexistence.

Values of χ/χ_c are, from top to bottom:
$\chi/\chi_c = \{1.102, 1.271, 1.695, 2.542, 3.390, 4.237, 5.085, 5.932, 6.780, 7.627, 8.475\}$.
Dashed line shows the function $-z/(2R_g) - (3R_g)/z$ for comparison (see text for explanation).

Figure 7: Characteristic lengths of the segregation profiles in units of the gyration radius, vs $1/(\chi N)$, in the symmetrical mixture at two phase coexistence. Solid line and long dashed line show the width of the profiles, defined in two different ways. Short dashed line gives asymptotic decay length ξ, dotted line gives half the interfacial width between the two coexisting phases in the bulk. Dashed dotted line indicates the extension of one undistorted chain in the bulk. Triangles mark the values of $1/(\chi N)$, corresponding to the profiles shown in Figs 6 and 9.

Figure 8: Distribution of chain end monomers of the minority component $\rho_{A,end}$ in units of $(2\rho_b/N)$ in the symmetric polymer mixture at two phase coexistence, $\chi/\chi_c = 1.696$. Dashed line indicates distribution of all monomers for comparison. Inset shows the total chain end distribution (solid line), compared to the total density profile (dashed line).

Figure 9: Logarithmic derivative of chain end distributions for the minority component in the symmetrical mixture, in units of R_g^{-1}, at two phase coexistence. Values of χ/χ_c are as in Figure 6, from top to bottom:
$\chi/\chi_c = \{1.102, 1.271, 1.695, 2.542, 3.390, 4.237, 5.085, 5.932, 6.780, 7.627, 8.475\}$.
Dashed line shows the function $-z/(2R_g) - R_g/z$

Figure 10: Profiles of the average squared z-component of the end-to-end vector $\langle R_{e,z}^2 \rangle$ for chains centered at z/R_g, vs z/R_g. Considered are chains of the minority component (dashed lines) and the majority component (solid line) in a symmetrical mixture at two phase coexistence, different values of χ. The results for chains of the majority component do not depend on χ.

Figure 11: Cartoon of a single weakly adsorbed chain in semi-infinite space

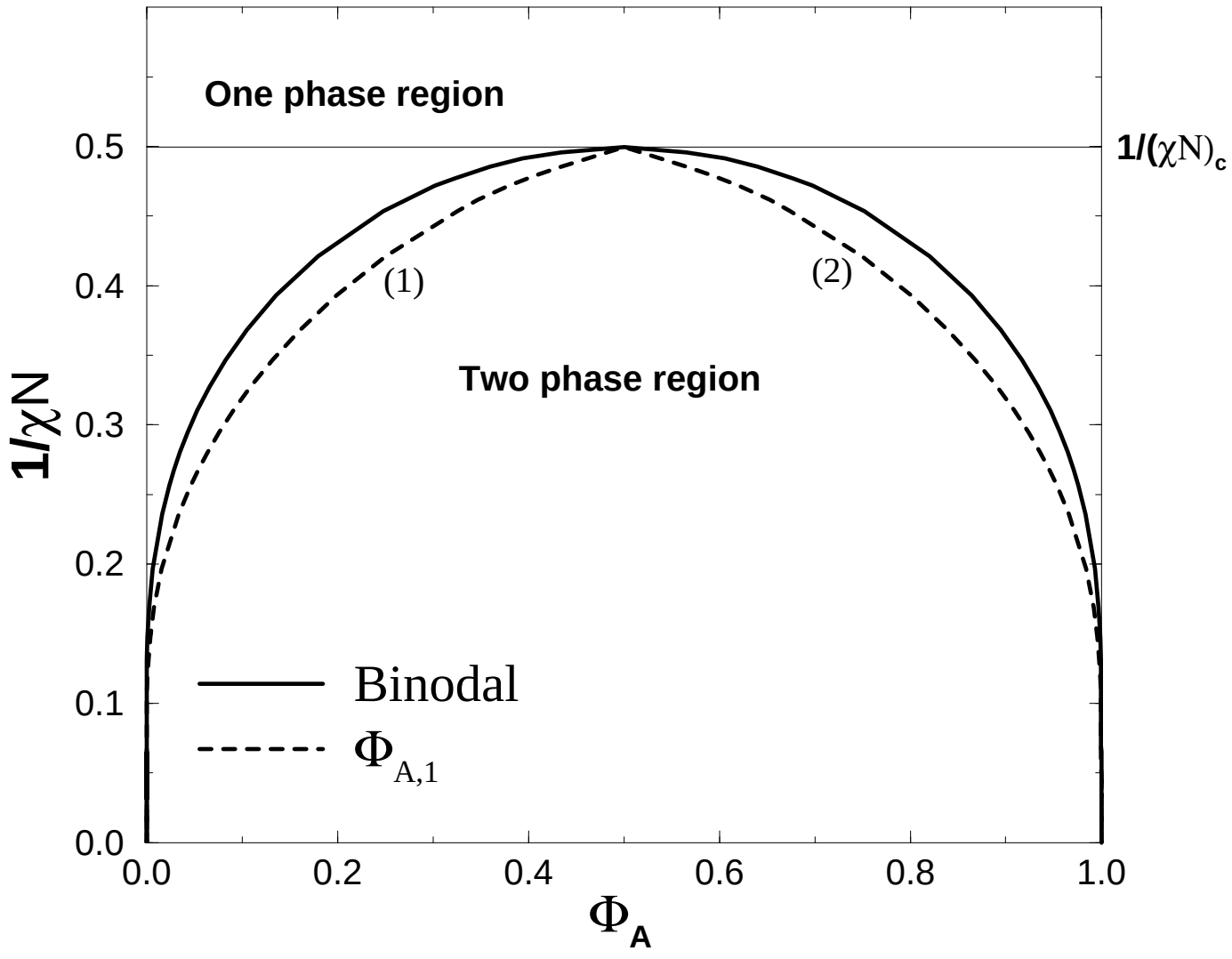
One phase region
Two phase region
(1)
(2)
1/(χN)c
1/χN
ΦA
Binodal
ΦA,1
0.0
0.1
0.2
0.3
0.4
0.5
0.0
0.2
0.4
0.6
0.8
1.0

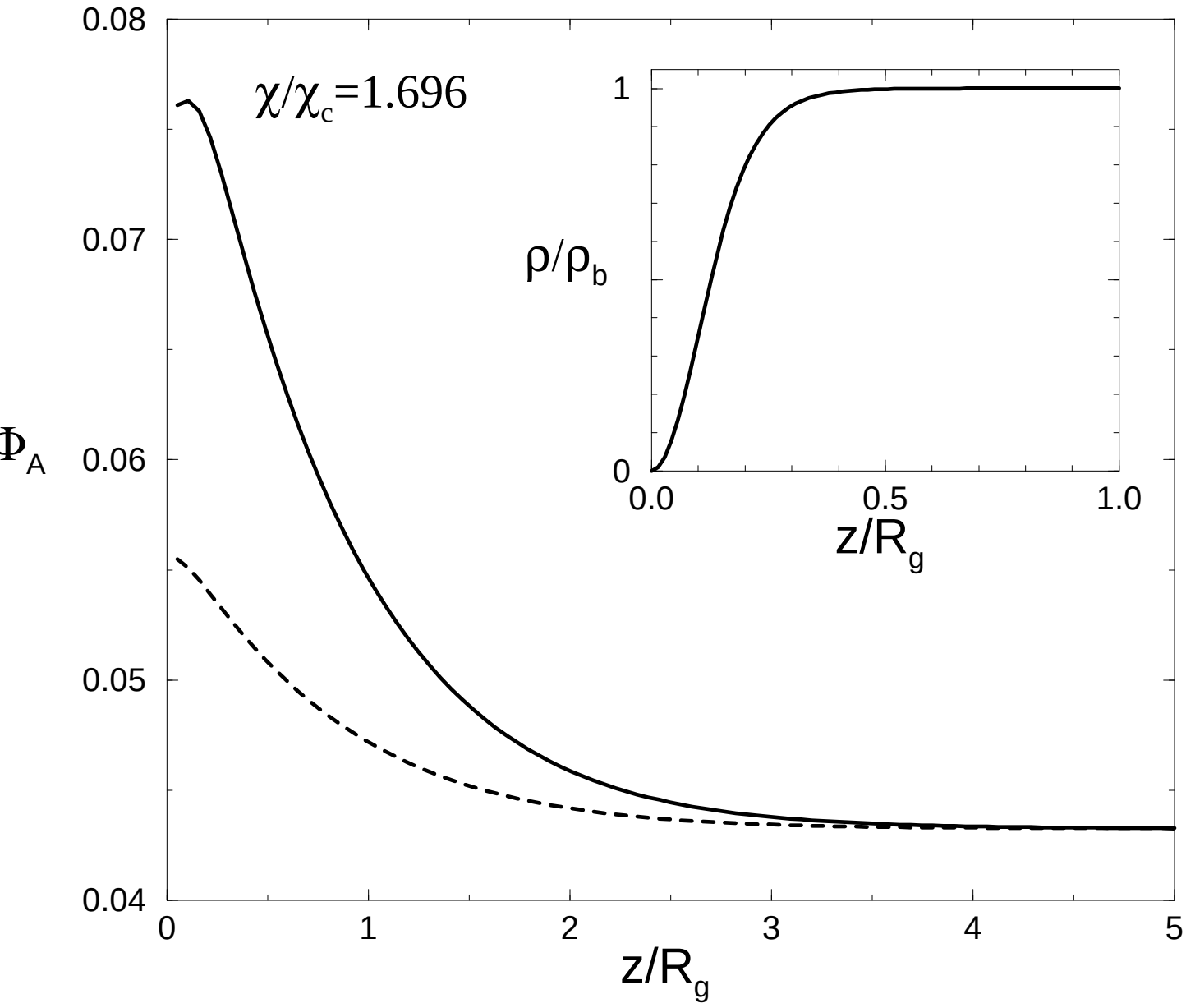
0.08
0.07
0.06
0.05
0.04
Φ_A
χ/χ_c=1.696
ρ/ρ_b
1
0
0.0
0.5
1.0
z/R_g
0
1
2
3
4
5
z/R_g

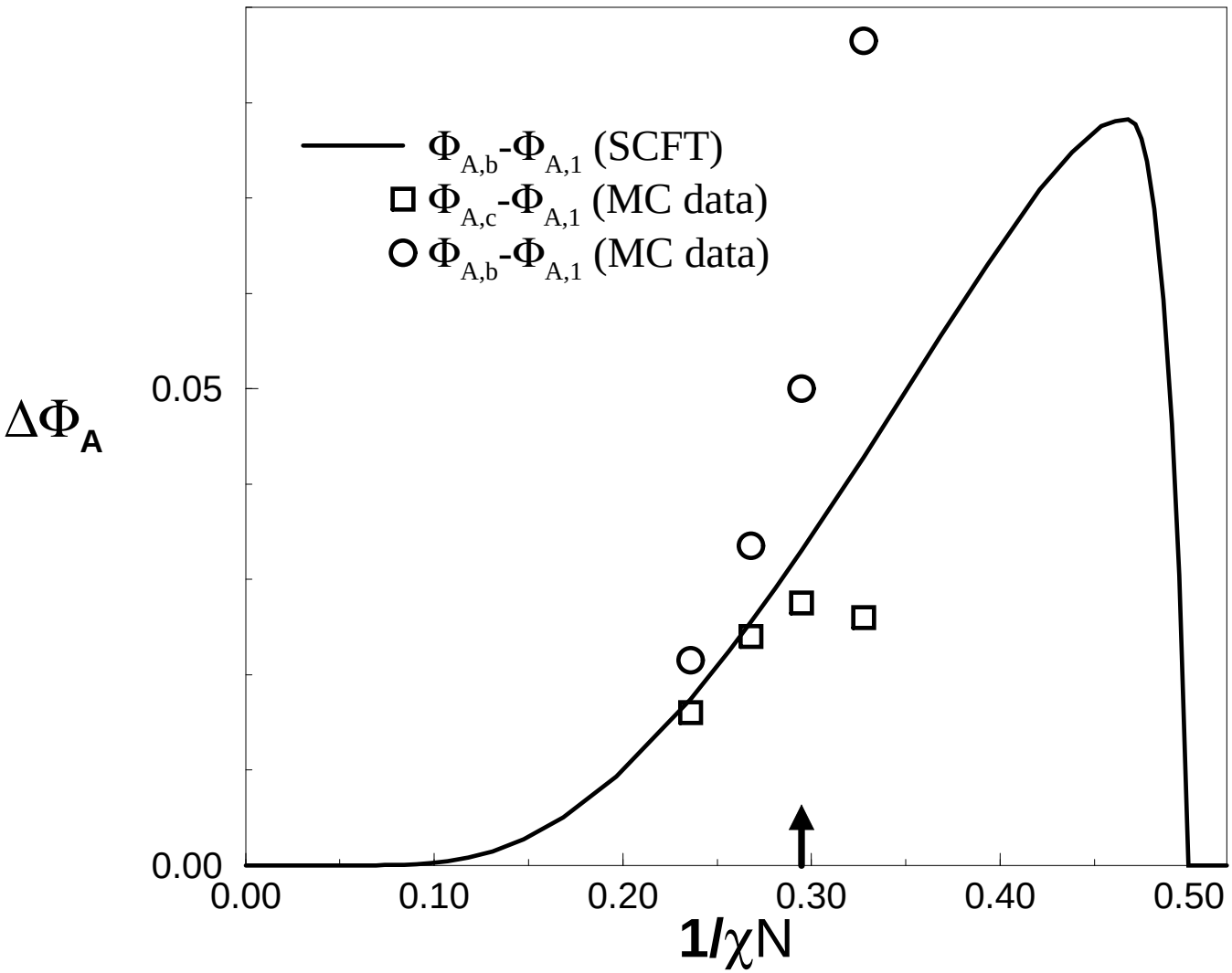
$\Phi_{A,b}$-$\Phi_{A,1}$ (SCFT)
$\Phi_{A,c}$-$\Phi_{A,1}$ (MC data)
$\Phi_{A,b}$-$\Phi_{A,1}$ (MC data)
$\Delta\Phi_A$
0.05
0.00
0.00
0.10
0.20
0.30
0.40
0.50
1/χN

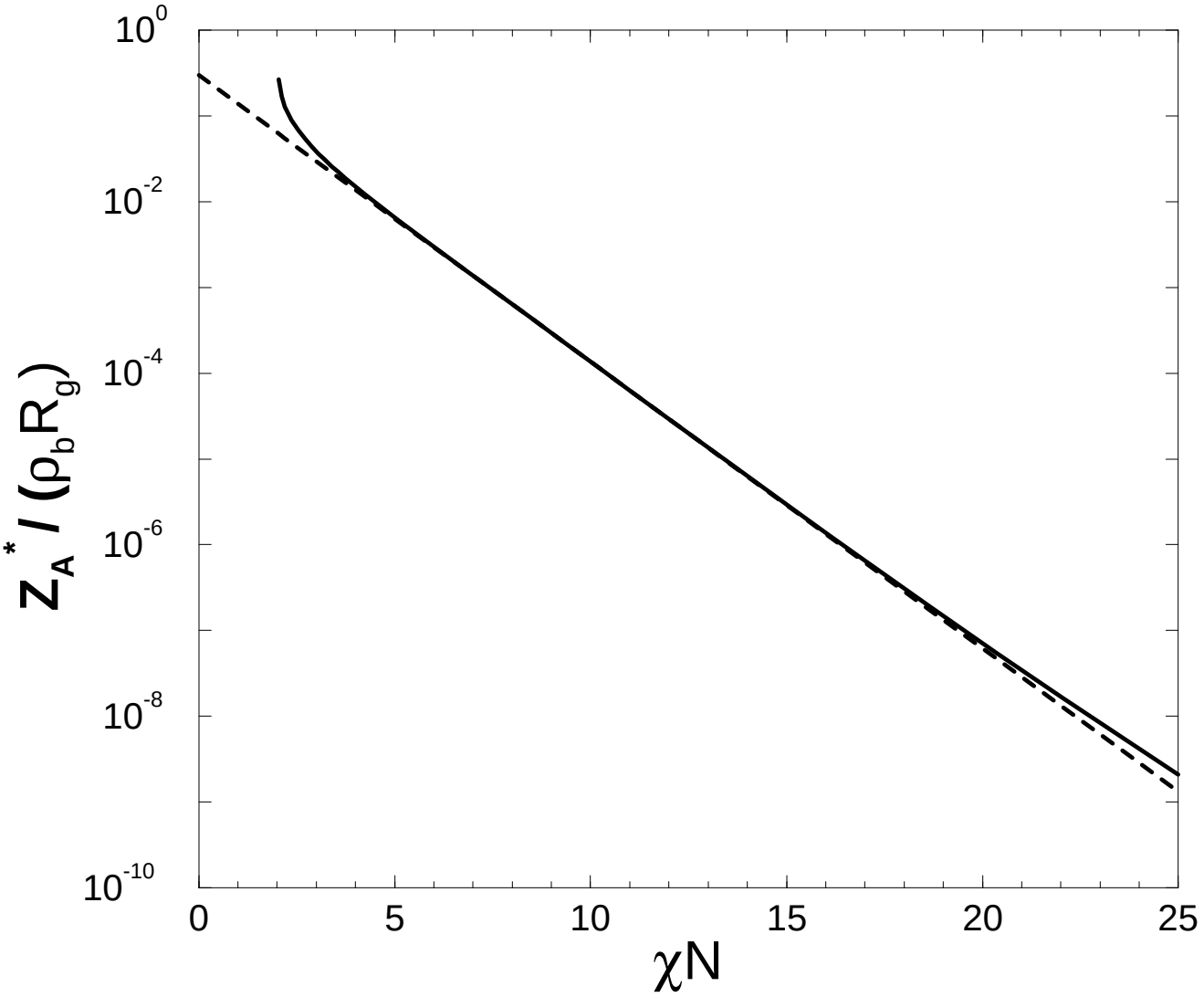
10^{0}
10^{-2}
10^{-4}
10^{-6}
10^{-8}
10^{-10}
$Z_A^* I / (\rho_b R_g)$
0
5
10
15
20
25
χN

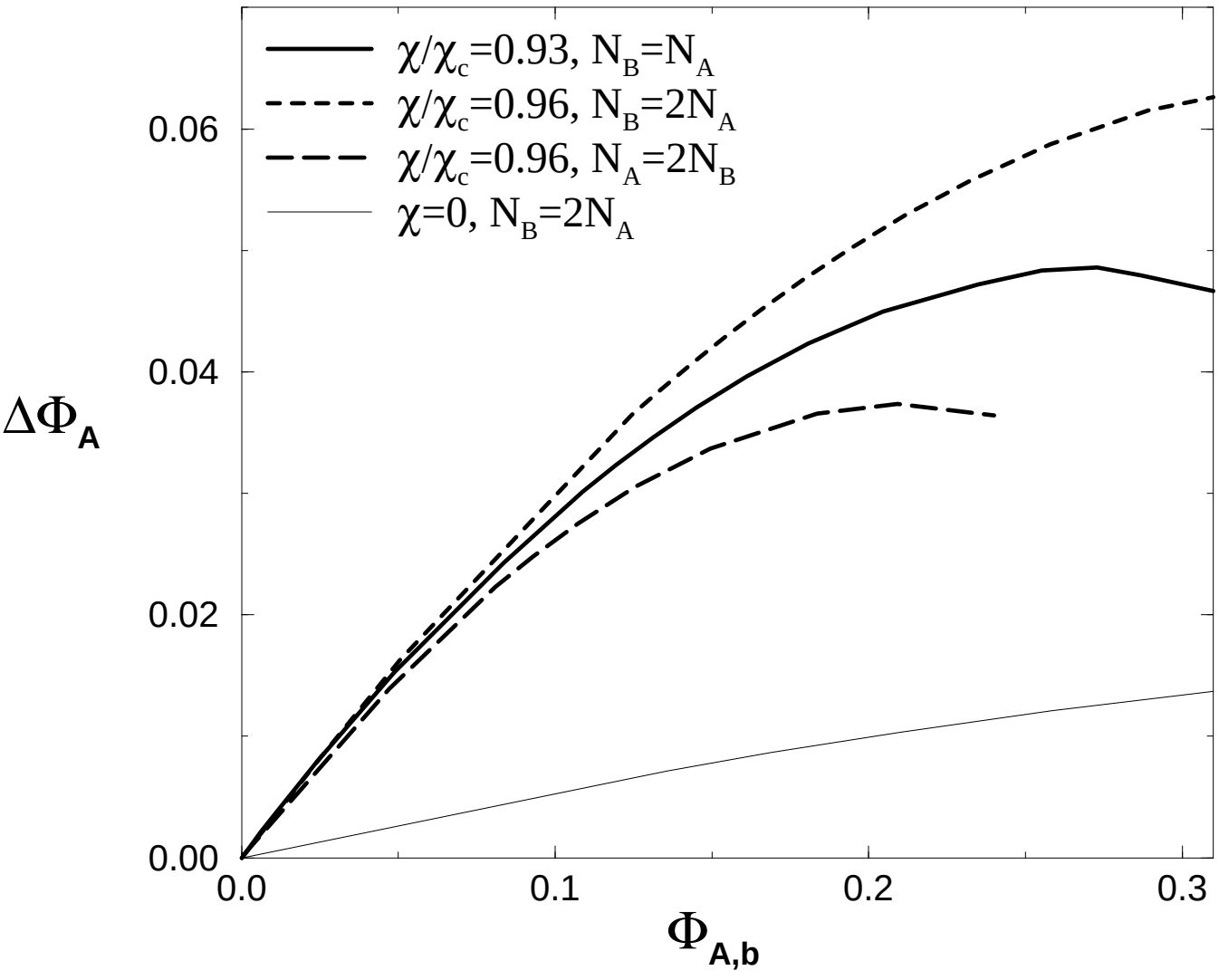
χ/χc=0.93, NB=NA
χ/χc=0.96, NB=2NA
χ/χc=0.96, NA=2NB
χ=0, NB=2NA
0.06
0.04
0.02
0.00
0.0
0.1
0.2
0.3
ΔΦA
ΦA,b

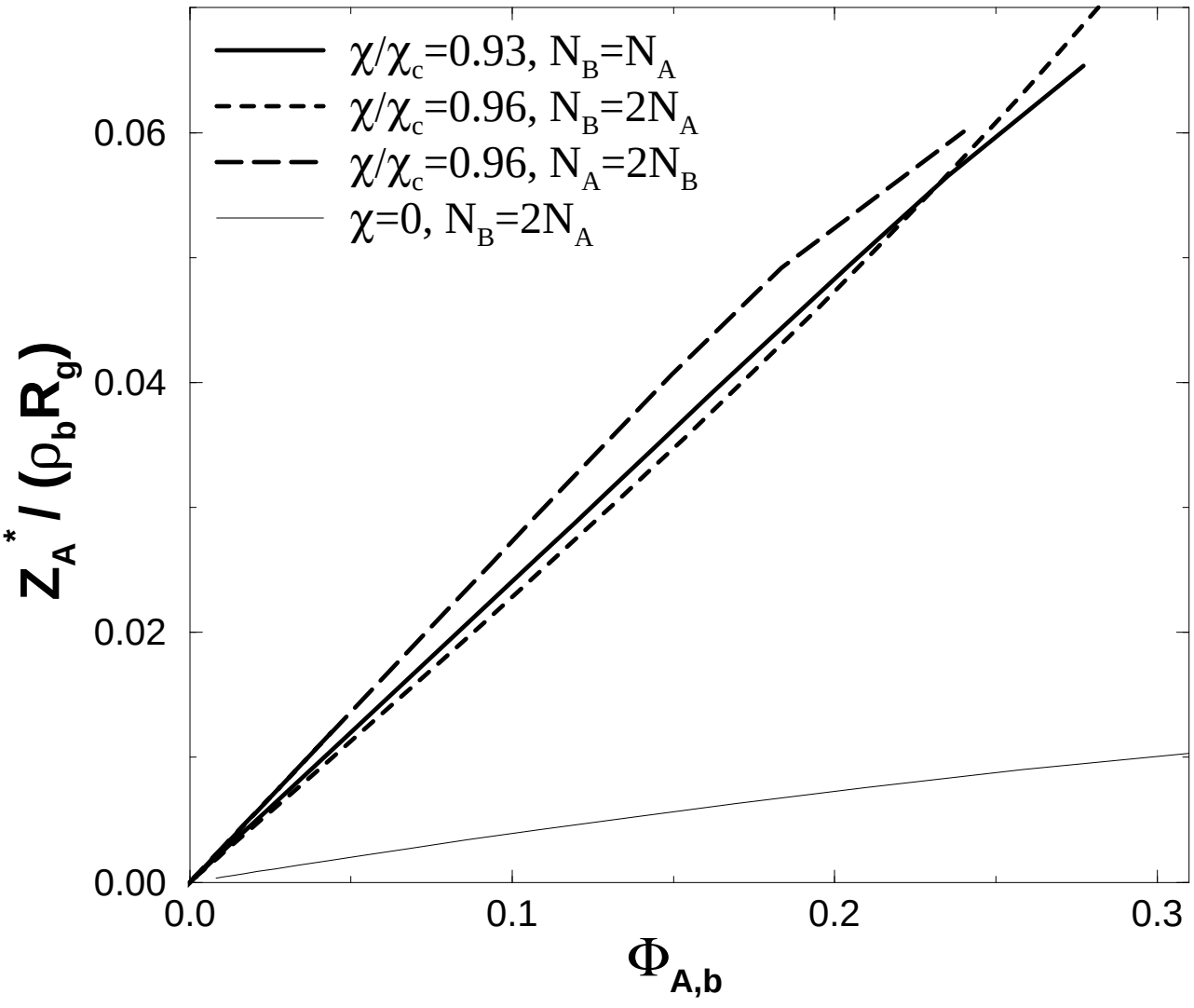
χ/χc=0.93, NB=NA
χ/χc=0.96, NB=2NA
χ/χc=0.96, NA=2NB
χ=0, NB=2NA
0.06
0.04
0.02
0.00
0.0
0.1
0.2
0.3
Z*A l (ρbRg)
ΦA,b

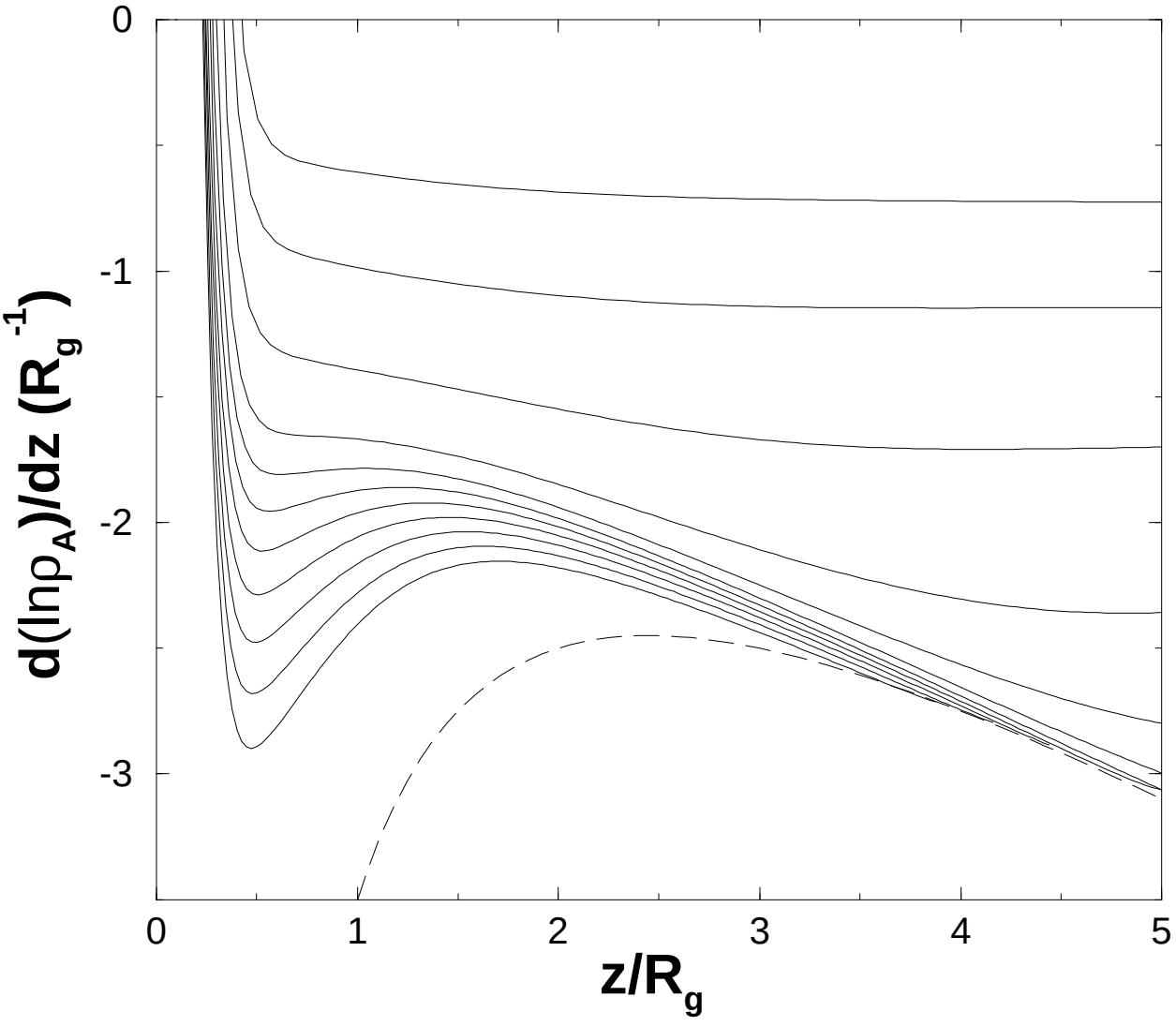
0
-1
-2
-3
0
1
2
3
4
5
d(lnρA)/dz (Rg-1)
z/Rg

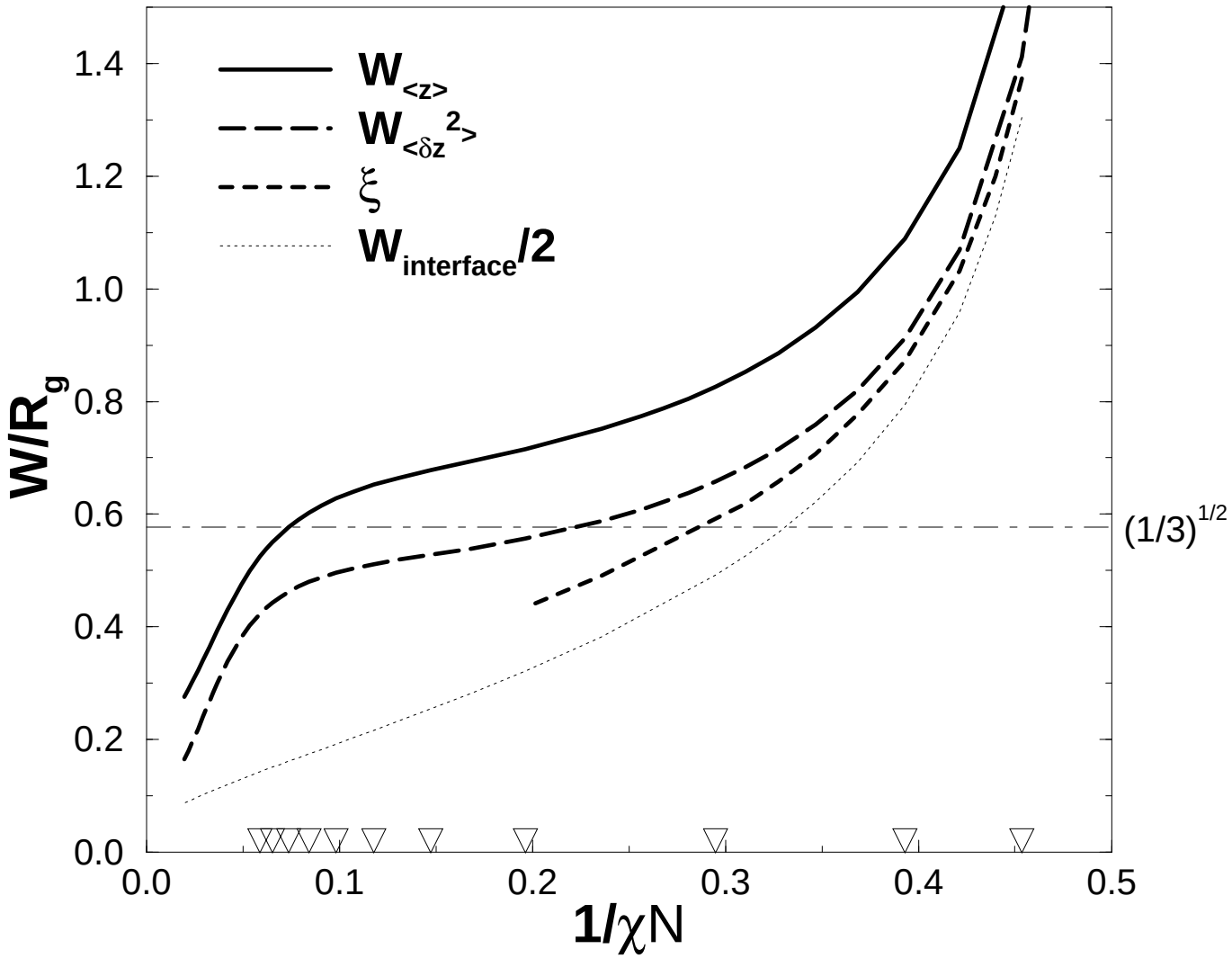
W<z>
W<δz2>
ξ
Winterface/2
W/Rg
1/χN
(1/3)1/2
0.0
0.2
0.4
0.6
0.8
1.0
1.2
1.4
0.1
0.3
0.5

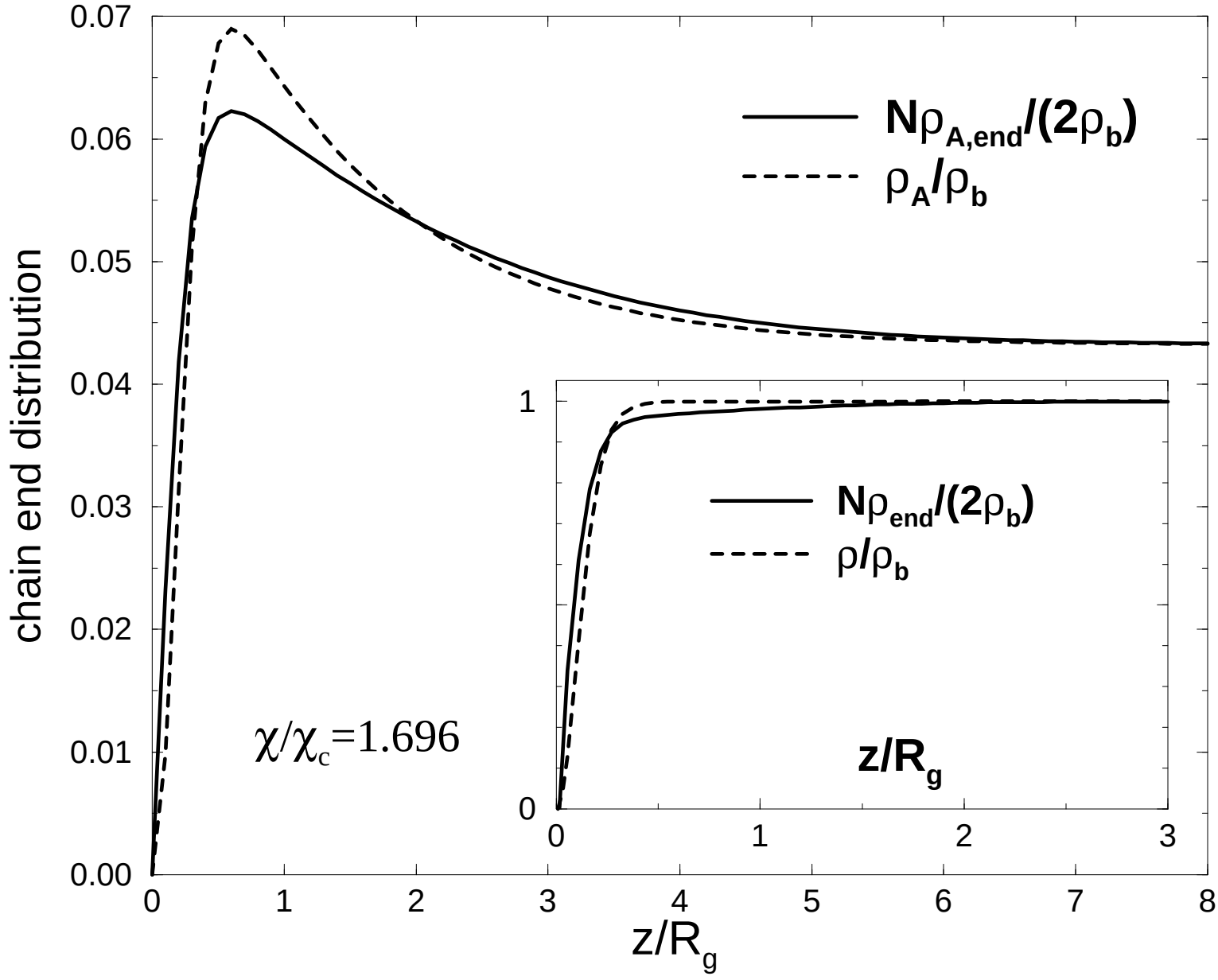
chain end distribution
z/R_g
Nρ_A,end/(2ρ_b)
ρ_A/ρ_b
χ/χ_c=1.696
Nρ_end/(2ρ_b)
ρ/ρ_b
z/R_g

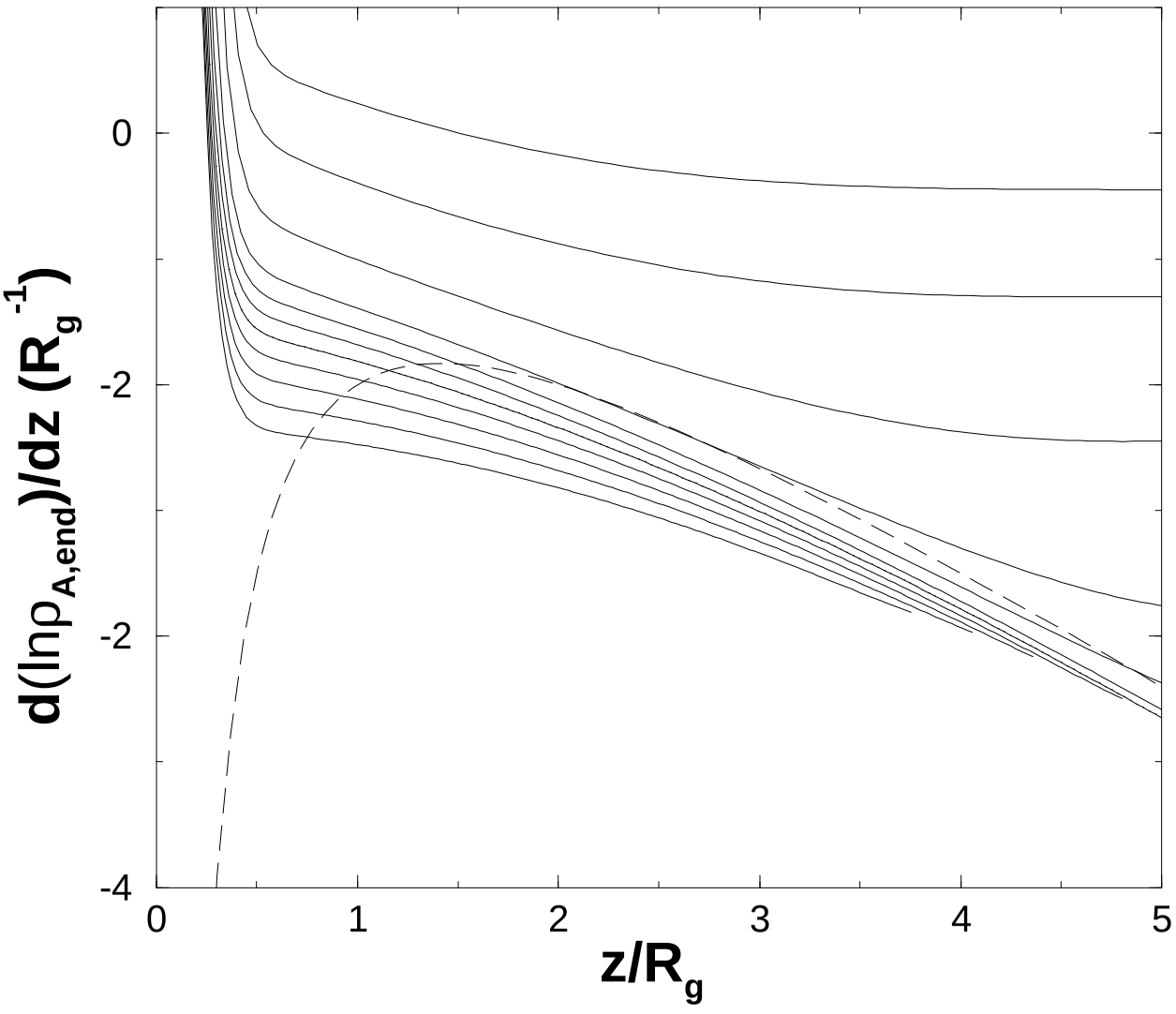
0
-2
-2
-4
0
1
2
3
4
5
d(lnρA,end)/dz (Rg-1)
z/Rg

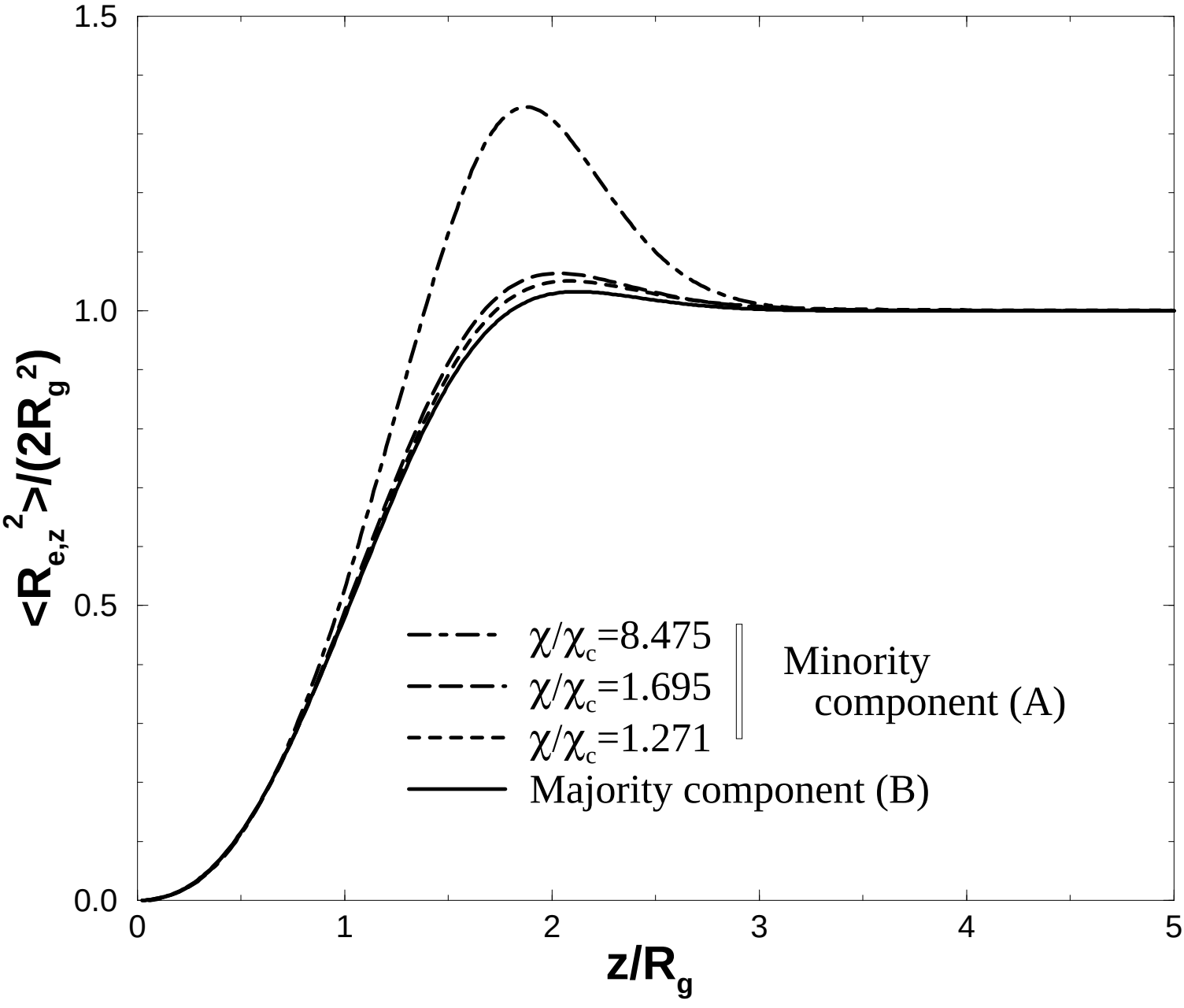
1.5
1.0
0.5
0.0
0
1
2
3
4
5
$<R_{e,z}^2>/(2R_g^2)$
z/R_g
χ/χ_c=8.475
χ/χ_c=1.695
χ/χ_c=1.271
Minority component (A)
Majority component (B)